Optimal Design Problem Formulation

In this chapter, generic issues relating to the optimal design of a vehicle propulsion system are briefly discussed, including the design objective and constraints. Furthermore, the problem of the optimal design for a vehicle propulsion system is formulated and solved through the bi-level and uni-level co-optimization approach.

7.1 Design Objective

Design of Vehicle Propulsion Systems (VPSs) is confronted with high complexities due to powertrain technology (conventional, battery-electric, or hybrid-electric vehicles), powertrain architecture (in particular, series, parallel, and power-split architecture for HEVs), powertrain component (mechanical and electrical ones, such as internal combustion engine, transmission, battery, electric motor/generator), powertrain control (powertrain control optimization for the minimal energy consumption in HEVs). Meanwhile new vehicle product offerings must concurrently response to meet customer wants and regulatory requirements. To cope with these complexities, the optimal design technique is highly requested to achieve the desired requirements, for instance, lower energy consumption.

Throughout this thesis, the objective of the optimal design problem for vehicle propulsion systems is solely to minimize the energy consumption by finding the best dimensioning parameters of powertrain components, which yields

$$\min_{d \in \mathcal{S}_{adm}} \mathcal{L}(d), \tag{7.1}$$

$$s.t. \quad g_i(d) \leq 0, \text{ for each } i \in \{1, \ldots, m\}, \tag{7.2}$$

$$h_j(d) = 0, \text{ for each } j \in \{1, \ldots, n\}, \tag{7.3}$$

where d presents generic dimensioning parameters to optimize that is defined by $d \in \left\{\mathcal{S} : \mathcal{S}_e \cup \mathcal{S}_d \cup \mathcal{S}_b \cup \mathcal{S}_m \cup \mathcal{S}_g\right\}$, $\mathcal{S}_{adm}$ is the admissible design space that is constrained by desired requirements, $\mathcal{L}(d)$ represents the energy consumption, and $g_i(d)$ and $h_j(d)$ indicate generic equality and in-equality constraints.

In particular, the objective function $\mathcal{L}(d)$ depends on powertrain technologies. Considering a conventional vehicle, the design objective function is

$$\mathcal{L}(d) = \int_{t_0}^{t_f} P_{ef}(t, d)\, dt; \tag{7.4}$$

whereas, the objective function for battery-electric vehicles is

$$\mathcal{L}(d) = \int_{t_0}^{t_f} P_{be}(t, d)\, dt. \tag{7.5}$$

The objective function of hybrid-electric vehicles is more complex than that of single-source ones because of the inevitability of control optimization for the evaluation of the minimal energy consumption. Thus, the objective function of the optimal design is

$$\mathcal{L}(d) = \int_{t_0}^{t_f} P_{ef}(u(t), t, d)\, dt. \tag{7.6}$$

7.2 Design Constraint

Constraints of the optimal design for vehicle propulsion systems are introduced and partially determined by the parameters of vehicle attributes, such as top speed, acceleration, and gradeability. Simple analytic models are developed to evaluate the design constraints based on the required vehicle attributes.

7.2.1 Vehicle Attribute

The considered constraints in the design problem of vehicle propulsion systems mainly consist of vehicle performance parameters, which are known as vehicle attributes. Despite comprehensive vehicle attributes discussed in [27], the most interesting ones are composed of vehicle top speed v_{top}, gradeability of start-up α_{ls} and of high speed α_{hs}, and standstill acceleration time from 0 to 100 km/h t_{100}. Apart from the aforementioned

parameters, all-electric range D is of high interest, particularly for plug-in hybrid-electric and battery-electric vehicles.

Top Speed

As a frequent mentioned vehicle attribute of light-duty vehicles, the top speed (denoted by v_{top}) is defined as a constant cruising speed that is determined by the available power and the resistance on a flat road.

The tractive effort is further simplified, because the energy consumption of the rolling friction is typically one order of magnitude smaller than the aerodynamic friction consumed power at vehicle top speed. Thus, the approximation of the maximum traction power for passenger cars is written as

$$P_{i,v} \approx \frac{\rho_{ar} C_{ar} A_{ar} v_{top}^3}{2}, \ (i = e, m), \tag{7.7}$$

where e indicates internal combustion engine in a conventional or hybrid-electric vehicle, whereas m refers to electric motor in a battery-electric or plug-in hybrid-electric vehicle.

Gradeability

Gradeability is a relevant metric for both light- and heavy-duty vehicles. It is defined as the grade which a vehicle can overcome at a certain speed. The approximated tractive effort of a vehicle climbing an uphill road with a slope α without accounting for powertrain efficiency is

$$T_{i,\alpha} = \frac{\left(m_v g C_{rr} \cos\alpha + m_v g \sin\alpha + 0.5 \rho_{ar} C_{ar} A_{ar} v_v^2\right) R_w}{\mathcal{R}_d}, \ (i = e, m), \tag{7.8}$$

where $\mathcal{R}_d$ is the dimensioning parameter of a drivetrain.

Correspondingly, the further simplified estimation of the maximum tractive power is

$$P_{i,\alpha} \approx m_v g v (\sin\alpha + C_{rr} \cos\alpha), \ (i = e, m). \tag{7.9}$$

In addition to the gradeability, a similar performance parameter, i.e. startability, is considered as well for both light- and heavy-duty vehicles [74]. The startability is only considered when a vehicle starts movement from standstill. Note that, the full load of vehicle is applied in both gradeability and startability estimation.

Acceleration Performance

The acceleration performance is usually described by the accelerating time from standstill to 100 km/h or to 60 mph and the distance covered from zero speed to a certain speed on level road. Using Newton's second law, the acceleration time t_{100} obtained from the maximum tractive effort is evaluated by

$$t_{100} = \int_0^{100/3.6} \frac{m_v}{T_i \mathcal{R}_d / R_w - m_v g C_{rr} - 0.5 \rho_{ar} C_{ar} A_{ar} v^2} \, dv. \tag{7.10}$$

The acceleration time from standstill to 100 km/h is not only valid for engine-based and hybrid-electric vehicles, but for some powerful battery-electric vehicles as well. Moreover, the acceleration time t_{100} is not able to compute directly due to the highly dynamic effects. A further simplified model between acceleration time and the maximal power of the main tractive powertrain component (such as internal combustion engine or electric motor/generator) is expressed as

$$t_{100} = c_{t100} \frac{m_v v_{100}^2}{P_{i,t}}, \ (i = e, m), \tag{7.11}$$

where $c_{t100} = 0.877$ for diesel engine vehicles, $c_{t100} = 0.929$ for gasoline engine vehicles, and $c_{t100} = 0.767$ for battery-electric vehicles.

A simple yet direct verification of the acceleration time model in Eq. 7.11 is demonstrated in Fig. 7.1 for conventional vehicles. The published acceleration time is denoted by t_{100}, whereas the estimated acceleration time is indicated by t_{100}^p. The estimated acceleration time agreed with the published one.

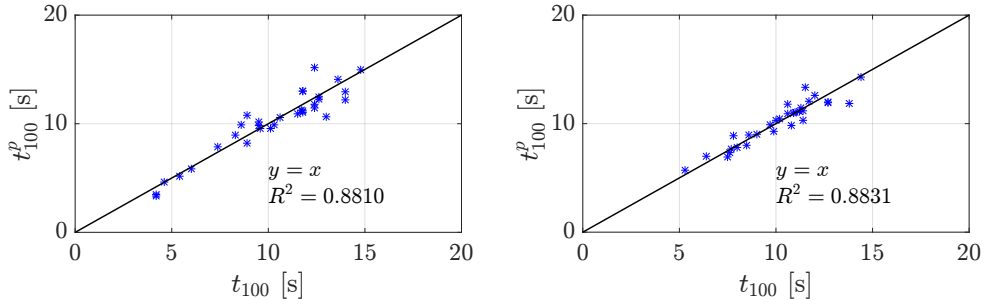

(a) gasoline engine (b) diesel engine

Figure 7.1 – Comparison of estimated and published acceleration time for conventional vehicles.

As for acceleration time of battery-electric vehicles, Fig. 7.2 shows the comparison between the estimated values and the published ones. Despite further simplified model in Eq. 7.11, the estimations of acceleration time agreed well with data.

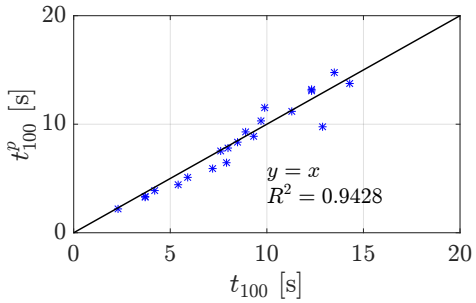

Figure 7.2 – Comparison of estimated and published acceleration time for battery-electric vehicles.

All-Electric Range

All-electric range is an essential design constraint for plug-in hybrid-electric and battery-electric vehicles. The all-electric range is determined by the applicable energy of battery and the specific energy consumption of a battery-electric vehicle, which yields

$$E_b = D \frac{\int_{t_0}^{t_f} P_{be}(t, d)\, dt}{\int_{t_0}^{t_f} v(t)\, dt}, \tag{7.12}$$

where E_b is the applicable energy of battery, D is the desired all-electric range.

7.2.2 Design Space

Design space is the admissible range of dimensioning parameters resulting from the design constraints. Vehicle attribute significantly affects the rated power and rated torque of the power sources, such as internal combustion engine, electric motor/generator.

As a consequence, the rated power of internal combustion engine or electric motor/-generator in different vehicle applications must satisfy

$$\mathcal{P}_i \geq \max\{P_{i,v}, P_{i,a}, P_{i,t}\}, \quad (i = e, m). \tag{7.13}$$

As for the rated torque of an internal combustion engine or electric motor/generator,

it is expressed as

$$\mathcal{T}_i \geq T_{i,\alpha}, \quad (i = e, m). \tag{7.14}$$

In regard to the desired all-electric range, the minimal applicable energy of a battery is constrained as

$$\mathcal{E}_b \geq E_b, \tag{7.15}$$

where $\mathcal{E}$ is the applicable energy of battery to size.

Additionally, implicit constraints on the dimensioning parameters of powertrain components are taken into account. For instance, battery must be capable of providing sufficient electrical power to electric motor/generator during vehicle operation. Considering an internal combustion engine, its rated torque is not independent from its displacement, which yields

$$\mathcal{T}_e = c_{et}\mathcal{V}_e, \tag{7.16}$$

where the coefficient c_{et} is 148.63 Nm/L for CI/TC engines, 161.81 Nm/L for SI/TC engines, and 93.44 Nm/L for SI/NA engines.

Furthermore, its torque of the rated power is linearly modeled as a function of engine displacement, which is given by

$$T_{ep} = c_{ep}\mathcal{V}_e, \tag{7.17}$$

where the coefficient c_{ep} is 116.34 Nm/L for CI/TC engines, 136.80 Nm/L for SI/TC engines, and 85.63 Nm/L for SI/NA engines.

Coefficients in Eq. 7.16 and 7.17 are further validated with the light-duty engines in Table 2.4. Fig. 7.3a, 7.4a, and 7.5a illustrate the comparison of the rated torque and the estimated one for engines in terms of SI/TC, SI/NA, and CI/TC, respectively; whereas the comparison of the torque of rated power is correspondingly depicted in Fig. 7.3b to 7.5b.

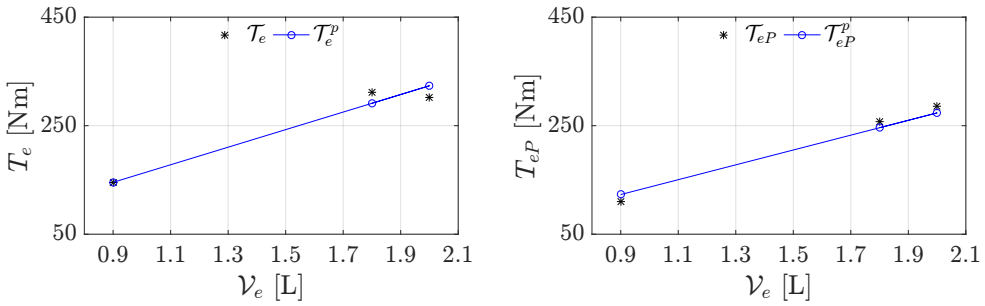

(a) rated torque (b) torque of rated power

Figure 7.3 – Comparison of rated torque and torque of rated power for SI/TC engines.

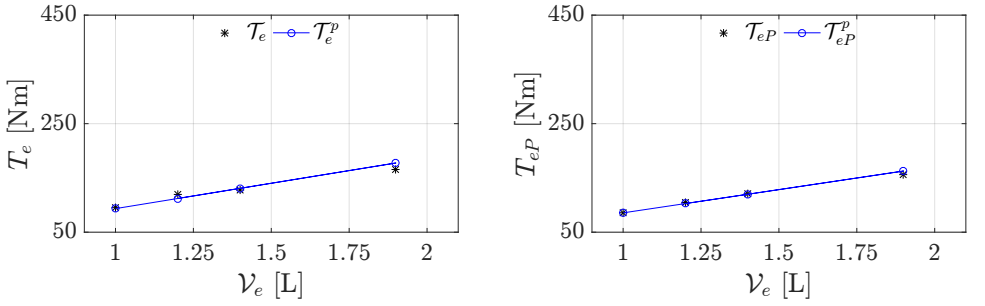

(a) rated torque (b) torque of rated power

Figure 7.4 – Comparison of rated torque and torque of rated power for SI/NA engines.

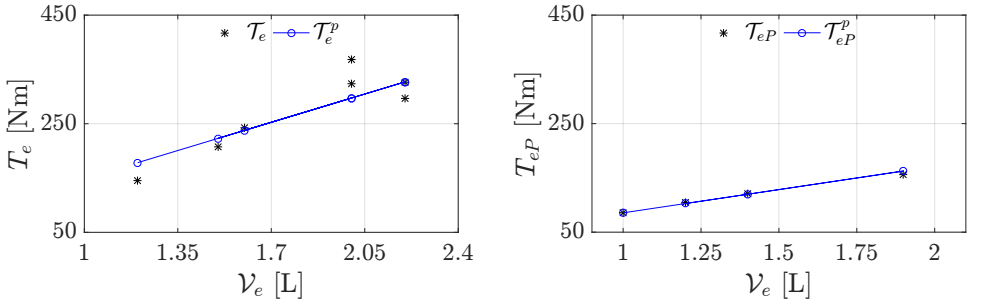

(a) rated torque (b) torque of rated power

Figure 7.5 – Comparison of rated torque and torque of rated power for CI/TC engines.

7.3 Design Method

The design optimization, particularly combining with control optimization for hybrid-electric vehicles, is commonly solved through a multidisciplinary system design optimization framework [75], for instance, through the bi-level co-optimization approach. As an alternative, the uni-level co-optimization approach is proposed as well, thanks to the development of FACE for hybrid-electric vehicles.

7.3.1 Bi-Level Co-Optimization Approach

Bi-level co-optimization approach is characterized by two optimizers that minimize the energy consumption at two distinct levels, in which are specifically for powertrain design and powertrain control. At the level of powertrain design, dimensioning parameters are optimized to get the global minimal fuel consumption; optimal powertrain control is applied to evaluate the minimum fuel consumption at the level of powertrain control for an investigated vehicle.

A flow chart of bi-level co-optimization approach is illustrated in Fig. 7.6. Dimensioning parameters are initialized and transferred to control optimizer. Then the minimal fuel consumption of vehicle propulsion systems is minimized by the design optimizer so that the optimal dimensioning parameters are determined. Once exit criteria are satisfied, the bi-level co-optimization process is completed and terminated. Due to two types of optimizations, the bi-level co-optimization approach is tailored for hybrid-electric vehicles.

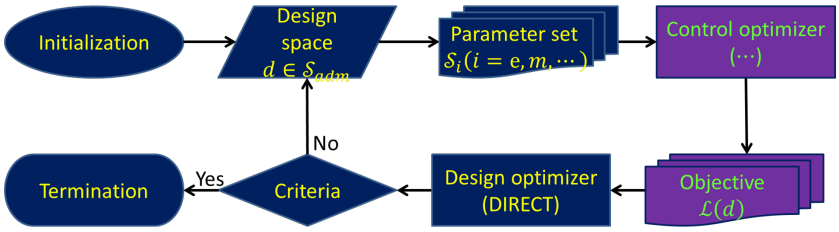

Figure 7.6 – Scheme of bi-level co-optimization approach.

The blue blocks in Fig. 7.6 represent operations relating to the powertrain design optimization in the outer loop; whereas the violet blocks are associated with the powertrain control optimization in the inner loop. Throughout this thesis, the design optimization is solely performed through DIRECT, whereas the control optimization is carried out by the methods presented in Chapter 4.

However, the bi-level co-optimization approach can be applied to single-source vehicles by replacing the powertrain control optimization with quasi-static simulation. Consequently, dimensioning parameters of single-source vehicles are optimized through the bi-level design optimization approach.

7.3.2 Uni-Level Co-Optimization Approach

As the development of FACE for single-source and hybrid-electric vehicles, the dimensioning parameter optimization can be regarded as a nonlinear programming problem, consisting of objective function (which is FACE) and general constraints (from the requirement of vehicle attributes).

By implementing FACE, the powertrain design optimization for hybrid-electric vehicles is performed in a uni-level co-optimization approach (see Fig.7.7) because powertrain control optimization is embedded in FACE. This uni-level co-optimization approach is much more complex compared with the bi-level co-optimization approach due to the high inherent nonlinearity of FACE, and the lack of suitable nonlinear solvers. However, the nonlinear solver is possibly replaced by simple method, such as the full space search method. Specific nonlinear solvers and optimization algorithms are introduced within corresponding case studies in Chapter 8.

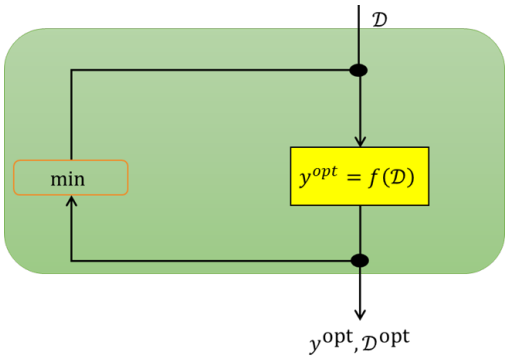

Figure 7.7 – Scheme of uni-level co-optimization approach.

Chapter 8

Optimal Design of Vehicle Propulsion Systems

Theories of analytic models of powertrain components, bi-level co-optimization, and uni-level co-optimization through FACE are applied to several case studies, including conventional, battery-electric and hybrid-electric vehicles. The energy consumption is always minimized by optimizing dimensioning parameters of powertrain components over specific missions through the bi-level co-optimization and the uni-level co-optimization approach.

8.1 Design Optimization of a Conventional Vehicle

The vehicle propulsion system of a reference conventional vehicle is optimized to further reduce energy consumption through the bi-level design optimization and uni-level design optimization approach. After the introduction of the main features of the powertrain and vehicle parameters, the optimal design problem describes the design constraints, resulting design space, and characteristics of design approaches. Results of optimized dimensioning parameters are comparatively presented and discussed.

8.1.1 Reference Vehicle

The main features of the reference conventional vehicle are listed in Table 8.1, including vehicle parameters [76], and dimensioning parameters of internal combustion engine and drivetrain in Table 2.4 and 2.7, respectively.

Vehicle	m_v [kg]	1595
	R_w [m]	0.308
	C_{v0} [N]	134.094
	C_{v1} [N/(m/s)]	3.7465
	C_{v2} [N/(m/s)^2]	0.3486
Engine	$\mathcal{I}_e$	CI/TC
	$\mathcal{V}_e$ [L]	2.15
	$\mathcal{T}_e$ [Nm]	292
	$\mathcal{P}_e$ [kW]	90
Drivetrain	$\mathcal{I}_t$	DCT-6
	$\mathcal{R}_{fd}$	4.12 & 3.04

Table 8.1 – Features of reference conventional vehicle.

8.1.2 Optimal Design Problem

The optimal design problem specifies the design constraints based on the reference conventional vehicle and the resulting design space. Moreover, the applied nonlinear solver in the uni-level co-optimization approach is specified in this case study.

Constraints

Based on the reference vehicle, design constraints consist of vehicle top speed, acceleration time from 0 to 100 km/h, and gradeability, which lead to

$$\begin{aligned} &\text{vehicle top speed in [km/h]}: && \geq 200\ , \\ &\text{acceleration time to 100 in [s]}: && \leq 13.5, \\ &\text{gradeability in [\%]}: && \geq 30. \end{aligned}$$

The dimensioning parameters to optimize are summarized by $\{\mathcal{I}_e,\ \mathcal{V}_e,\ \mathcal{I}_t\}$, where $\mathcal{I}_e$ contains SI/NA/SB, SI/NA/LB, and CI/TC; $\mathcal{I}_t$ includes six-speed manual and automated transmission. Moreover, technological parameters $\mathcal{I}_e$ and $\mathcal{I}_t$ are represented by integers corresponding to different technologies.

Based on the desired top speed, the rated power of engine is initially constrained according to Eq. 7.1b. By combining Eq. 7.16 and 7.17, the minimum engine displacement of each engine technology is estimated, thus leading to the overall minimum of engine displacement $\mathcal{V}_e \geq 1.82$ L.

As for the transmission technological parameter $\mathcal{I}_t$, the ratio of last gear $\mathcal{R}_{tk}$ is determined by the required top speed; whereas the ratio of first gear $\mathcal{R}_{t1}$ is determined by the engine displacement and the required gradeability.

Approaches

Both approaches of bi-level and uni-level design optimization are implemented to optimize dimensioning parameters of powertrain components. DIRECT is applied in the bi-level design optimization approach.

Considering the uni-level design optimization, a nonlinear solver is applied to minimize the objective functional, which is FACE. As a nonlinear programming problem, the uni-level optimization is solved by the function "fmincon" in MATLAB. However, "fmincon" cannot handle the integer design parameters. Therefore, the uni-level design optimization repeats all the combinations of the integer parameters, which are the technological parameters of engine and transmission.

8.1.3 Result and Discussion

The optimized dimensioning parameters are reported in terms of bi-level and uni-level design optimization. In addition, the impact of missions on the optimal dimensioning parameters are investigated and discussed as well.

Impact of Optimization Approach

The reference vehicle is optimized separately through the bi-level design optimization (with quasi-static simulation in the inner loop) and the uni-level design optimization (with FACE) over NEDC. Because of implementation of QSS, results of the bi-level design optimization approach are denoted by QSS in this whole chapter. On the other hand, FACE is used to indicate the results of the uni-level design optimization approach.

As illustrated in Fig. 8.1, results of fuel consumption based on bi-level and uni-level design optimization are compared with the fuel consumption of the reference vehicle. About 8.27% of fuel consumption was saved by optimizing the design parameters of powertrain components over NEDC. Furthermore, both optimization approaches obtained the same improvement on fuel consumption.

In addition, the optimal dimensioning parameters are listed in Table 8.2, where VehR, VehNb, and VehNu stand for the reference conventional vehicle, optimized powertrain through the bi-level design optimization, and through the uni-level design optimization, respectively. Considering the results of the uni-level design optimization, the optimal design problem was solved by a nonlinear solver "fmincon" under the assumption that the initial solution referred to the reference vehicle. The initial solution did not affect the optimal solution of dimensioning parameters due to the convexity of FACE for conventional vehicles. Despite the restriction of integers, uni-level design optimization

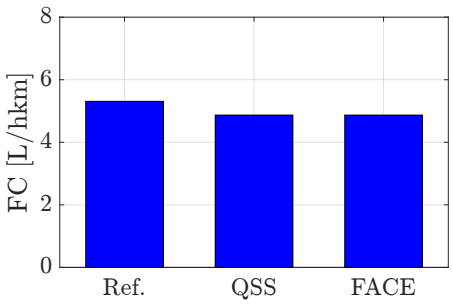

Figure 8.1 – Energy consumption of optimized and reference conventional vehicles over NEDC.

presented the same results of optimal dimensioning parameters as the bi-level design optimization.

	$\mathcal{I}_e$	$\mathcal{V}_e$ [L]	$\mathcal{T}_e$ [Nm]	$\mathcal{P}_e$ [kW]	$\mathcal{I}_t$	$\mathcal{R}_{t1}$	$\mathcal{R}_{t6}$
VehR	CI/TC	2.25	292	90	MT-6	14.25	2.31
VehNb	CI/TC	1.82	270	89	MT-6	11.39	2.26
VehNu	CI/TC	1.82	270	89	MT-6	11.39	2.26

Table 8.2 – Dimensioning parameters of optimized conventional vehicles via bi- and uni-level optimization approach based on NEDC.

Additionally, comparison of vehicle performance between the reference and the optimized one is presented in Table 8.3. With further reduced fuel consumption, the optimized vehicle propulsion system had a slightly higher top vehicle speed, poorer acceleration time, and lower gradeability. Nevertheless, both performance parameters satisfied the design constraints. The history of acceleration from 0 to 100 km/h is illustrated in Fig.8.2, where the initial acceleration capability of the optimized vehicle was worse than the reference one.

	V_{top} km/h	t_{100} [s]	α [%]
VehR	197	9.6	63.99
VehN	201	11.6	42.39

Table 8.3 – Vehicle performance of optimized conventional vehicle compared with reference one.

Concerning computation time, the bi-level design optimization needed about 44 min to complete the entire optimization process with 20 iterations and 447613 function evaluations; whereas, the uni-level design optimization only took about 0.56 s with 9

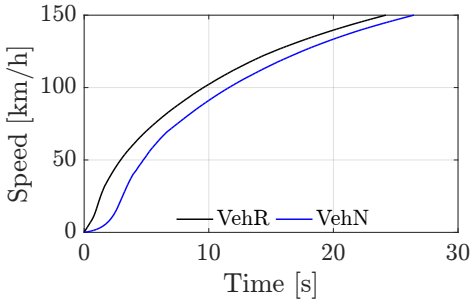

Figure 8.2 – Acceleration performance of optimized and reference conventional vehicles.

iterations and 22 function evaluations. Obviously, the uni-level design optimization significantly decreased the computation time compared with bi-level design optimization approach.

Impact of Mission

Under the same design considerations, the reference vehicle is optimized via the uni-level design optimization approach over two other missions, which are FTP-72 and HYWFET.

Results of the energy consumption of each optimized vehicle propulsion system are illustrated in Fig. 8.3. The largest improvement of energy consumption (about 9%) was achieved by the optimized vehicle over FTP-72 (VehF); while the least (about 3%) was obtained by that over HYWFET (VehH). However, the optimized dimensioning parameters of different missions are identical to each other as summarized in Table 8.4. Thus, missions did not affect the optimal dimensioning parameters.

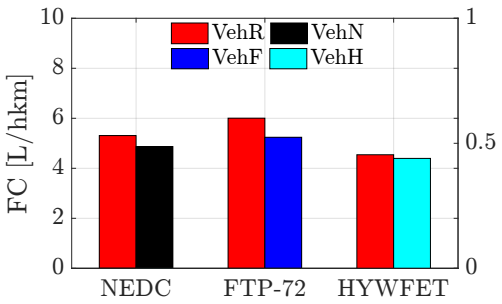

Figure 8.3 – Energy consumption of optimized conventional vehicles over different missions.

	$\mathcal{I}_e$	$\mathcal{V}_e$ [L]	$\mathcal{T}_e$ [Nm]	$\mathcal{P}_e$ [kW]	$\mathcal{I}_t$	$\mathcal{R}_{t1}$	$\mathcal{R}_{t6}$
VehN	CI/TC	1.82	270	89	MT-6	11.39	2.26
VehF	CI/TC	1.82	270	89	MT-6	11.39	2.26
VehH	CI/TC	1.82	270	89	MT-6	11.39	2.26

Table 8.4 – Dimensioning parameters of optimized conventional vehicles based on various missions.

8.2 Design Optimization of a Battery-Electric Vehicle

Both bi-level and uni-level design optimization are applied to minimize the electrical energy consumption of a reference battery-electric vehicle, therefore enlarging the all-electric range. The investigated dimensioning parameters are associated with battery and electric motor/generator. The structure of this case study is maintained the same as previous one, which consists of the introduction of a reference vehicle, further explanation of optimal design problem, and result discussion.

8.2.1 Reference Vehicle

Table 8.5 reports the main features of the reference battery-electric vehicle, consisting of vehicle parameters [77], dimensioning parameters of battery, electric motor/generator, and drivetrain. The battery and electric motor/generator are referred to the identification sets in Table 2.10 and 2.14, respectively. A single-speed transmission is installed in the drivetrain.

Vehicle	m_v [kg]	1648
	R_w [m]	0.3017
	C_{v0} [N]	141.9465
	C_{v1} [N/(m/s)]	1.1530
	C_{v2} [N/(m/s)^2]	0.3952
Battery	$\mathcal{I}_b$	HE
	$\mathcal{Q}_b$ [Ah]	31
	$\mathcal{K}_b$	192
Electric Motor	$\mathcal{I}_m$	PMSM
	$\mathcal{T}_m$ [Nm]	108
	$\mathcal{P}_m$ [kW]	78
Drivetrain	$\mathcal{R}_d$	14

Table 8.5 – Features of reference battery-electric vehicle.

8.2.2 Optimal Design Problem

Specific design constraints of the reference battery-electric vehicle are introduced with the resulting design space of the investigated dimensioning parameters. Further explanations regarding to the optimal design problem are given the clarify the powertrain design optimization, especially the uni-level design optimization.

Constraints

Based on the reference battery-electric vehicle, the technical targets, including top vehicle speed, acceleration time from 0 to 100 km/h, gradeability, and all-electric range are summarized as

$$\begin{aligned} &\text{vehicle top speed in [km/h]:} && \geq 140\ , \\ &\text{acceleration time to 100 in [s]:} && \leq 13.5, \\ &\text{gradeability in [\%]:} && \geq 25, \\ &\text{all-electric range in [km]:} && \geq 130. \end{aligned}$$

The investigated dimensioning parameters are listed in $\{\mathcal{Q}_b,\ \mathcal{K}_b,\ \mathcal{T}_m,\ \mathcal{N}_m\}$, where $\mathcal{Q}_b$ and $\mathcal{N}_b$ are integer parameters. The battery cells of high-energy type are considered only because of better all-electric range, although another type of battery cell can also be investigated.

According to the constraint of top vehicle speed, the lower boundary of the rated power of electric motor is calculated by Eq. 7.11. Concerning the gradeability, the lower boundary of the rated torque of electric motor is evaluated through Eq. 7.8. The base speed of electric motor is within the base speeds of identification set of electric motor/generators in Table 2.14. As for their upper boundaries, random values are chosen without losing fidelity.

As for the battery, capacity of cells is referred to the identification set of battery of high-energy type in Table 2.11. Note that, the upper boundary is limited to 53 Ah for the sake of consistent predictive analytic models. The battery-cell number $\mathcal{K}_b$ is randomly chosen but meet the requirement of all-electric range. In addition, battery must provide sufficient power to propel the electric motor/generator. Consequently, resulting design space are

$$\mathcal{Q}_b \in [25,\ 53], \tag{8.1}$$

$$\mathcal{K}_b \in [90,\ 285], \tag{8.2}$$

$$\mathcal{T}_m \in [110,\ 277], \tag{8.3}$$

$$\mathcal{N}_m \in [4000,\ 8500], \tag{8.4}$$

$$\mathcal{P}_m \in [73,\ 150]. \tag{8.5}$$

Although no additional constraints are considered, battery terminal power has been cross-verified to meet the requirement of acceleration and the operating limits over investigated missions.

Approaches

Both approaches of the bi-level and uni-level design optimization are implemented to optimize the mentioned dimensioning parameters of battery and electric motor/generator. The bi-level design optimization in done by DIRECT as the one in the previous case.

Regarding the uni-level design optimization, a new method of full-space search, instead of the "fmincon" function of MATLAB, is applied to optimize the dimensioning parameters. The reason is due to the higher nonlinearity of FACE for battery-electric vehicles than that for conventional vehicles.

Based on discretization of the design space, the full-space search method minimizes the energy consumption through multi-dimensional array operation that is effective for limited quantity of dimensioning parameters.

8.2.3 Result and Discussion

The optimized dimensioning parameters are summarized in terms of the bi-level and uni-level design optimization. In addition, the impact of missions on the optimized dimensioning parameters are investigated and discussed.

Impact of Optimization Approach

Fig. 8.4 compares the minimal energy consumption of the optimized vehicle through the bi-level (denoted by QSS) and the uni-level design optimization approach (indicated by FACE). Both the bi-level and uni-level design optimization reduced the minimal energy consumption to the same level, which was about 7.4% less than that of the reference vehicle.

As listed in Table 8.6, the optimal dimensioning parameters via the bi-level (marked by VehNb) and the uni-level design optimization (marked by VehNu) are compared with the ones of the reference vehicle (VehR). The optimized dimensioning parameters

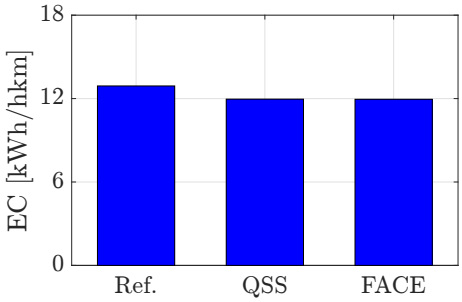

Figure 8.4 – Energy consumption of reference and optimized battery-electric vehicles over NEDC.

of VehNb and VehNu were almost the same to each other. The slight difference were probably caused by the discretization of the design space.

Compared with the reference vehicle, the battery capacity was increase to the upper boundary due to the lowest internal resistance of battery cells. Larger sizes of electric motor/generator were chosen because of the improved operating efficiency. For example, the electrical energy of electric motor in propulsion was reduced about 7% with respect to the reference vehicle.

	$\mathcal{Q}_b$ [Ah]	$\mathcal{K}_b$	$\mathcal{T}_m$ [Nm]	$\mathcal{P}_m$ [kW]	$\mathcal{N}_m$ [rpm]
VehR	31	192	108	79	6985
VehNb	53	113	274	150	5232
VehNu	53	110	277	150	5163

Table 8.6 – Dimensioning parameters of optimized battery-electric vehicles via bi- and uni-level optimization approach based on NEDC.

A comparison of vehicle performance between the reference vehicle (VehR) and the optimized vehicle (VehN) is listed in Table 8.7. The optimized vehicle had similar top speed and all-electric range, but further enhanced gradeability and acceleration performance. The history of acceleration from 0 to 100 km/h is depicted in Fig.8.5 for both the reference and optimized vehicle, where a larger size of electric motor/generator improved the acceleration performance.

The computation time of the bi-level design optimization was about 12.7 s with 100 iterations and 2995 function evaluations. However, the computation time of the uni-level design optimization through multi-dimensional array operation only took 1.25 s, which was an improvement of one order of magnitude.

	V_{top} [km/h]	t_{100} [s]	α [%]	All-Electric Range [km]
VehR	143	12.4	21.2	134
VehN	143	5.6	64.0	133

Table 8.7 – Vehicle performance of optimized battery-electric vehicle compared with reference one.

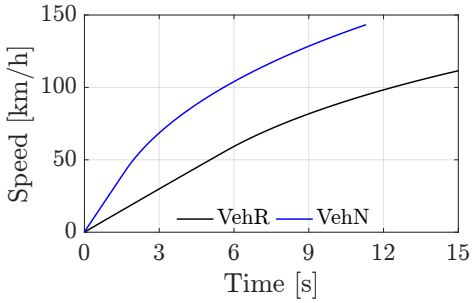

Figure 8.5 – Acceleration performance of optimized and reference battery-electric vehicle.

Impact of Mission

The reference vehicle is optimized based on two other missions through the bi-level design optimization, in order to verify the impact of missions.

As illustrated in Fig. 8.6, the minimized energy consumption is compared between the optimized vehicles and the reference one. Apart from VehR and VehN, VehF and VehH represented the optimized vehicle based on FTP-72 and HYWFET, respectively. Among all of the optimized vehicles, the largest reduction of 7.4% was achieved by the one over NEDC; whereas the least energy consumption reduction of 3.5% was achieved over HYWFET.

The optimization of vehicle propulsion system design was affected by missions. The optimized vehicle VehN presented similar energy consumption to the other mission-dependent optimized vehicles. This is probably due to NEDC combines the urban and extra-urban driving conditions.

Table 8.8 summarizes the optimal dimensioning parameters over the investigated missions. The mission influenced the optimal dimensioning parameters of battery. However, the dimensioning parameters of electric motor/generator were almost maintained the same, since they were heavily affected by the design constraints.

Based on the optimized dimensioning parameters in Table 8.8, the performance of the optimized vehicles are summarized in Table 8.9. The significant difference was

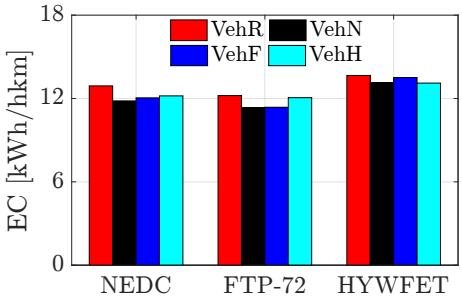

Figure 8.6 – Energy consumption of optimized battery-electric vehicles over different missions.

	$\mathcal{Q}_b$ [Ah]	$\mathcal{K}_b$	$\mathcal{T}_m$ [Nm]	$\mathcal{P}_m$ [kW]	$\mathcal{N}_m$ [rpm]
VehN	53	113	274	150	5232
VehF	53	121	261	150	5473
VehH	35	285	274	150	5232

Table 8.8 – Dimensioning parameters of optimized battery-electric vehicles based on various missions.

the all-electric-range due to the applicable energy of battery and the specific energy consumption.

	V_{top} [km/h]	t_{100} [s]	α [%]	All-Electric Range [km]
VehN	143	5.6	64.0	133
VehF	143	5.7	60.0	150
VehH	143	5.6	64.0	221

Table 8.9 – Vehicle performance of optimized battery-electric vehicles based on various missions.

8.3 Co-Optimization of a Series Hybrid-Electric Truck

VHOT, GRAB-ECO, and FACE are applied to optimize the dimensioning parameters of the propulsion system of a series hybrid-electric truck for better fuel savings.

8.3.1 Reference Vehicle

As reported in Table 8.10, the main features of the reference vehicle are summarized including vehicle parameters, internal combustion engine, electric generator, battery,

and electric motor.

Vehicle	m_v [kg]	13500
	R_w [m]	0.44
Engine	$\mathcal{I}_e$	CI
	$\mathcal{V}_e$ [L]	4.8
	$\mathcal{T}_e$ [Nm]	818
	$\mathcal{P}_e$ [kW]	167
Electric Generator	$\mathcal{I}_g$	PMSM
	$\mathcal{T}_g$ [Nm]	400
	$\mathcal{P}_g$ [kW]	70
Battery	$\mathcal{I}_b$	LiB
	$\mathcal{Q}_b$ [Ah]	138
	$\mathcal{K}_b$	48
Electric Motor	$\mathcal{I}_m$	AIM
	$\mathcal{T}_m$ [Nm]	450
	$\mathcal{P}_m$ [kW]	103

Table 8.10 – Main features of investigated series hybrid-electric vehicle.

8.3.2 Co-Optimization Problem

Constraints

In comparison with light-duty vehicles, vehicle attributes of heavy-duty vehicles are not explicit, except for the gradeability. Powertrain dimensioning parameters of the reference series hybrid-electric truck is optimized without considering any extra requirements of vehicle attributes. The design objective is to minimize fuel consumption of the reference powertrain over the real-world driving cycles.

The investigated dimensioning parameters include $\left\{\mathcal{R}_g,\ \mathcal{K}_b,\ \mathcal{T}_m, \mathcal{P}_m\right\}$, where battery number $\mathcal{K}_b$ is an integer parameter. Without taking extra vehicle attributes into account, the dimensioning parameters of $\mathcal{R}_g$ and $\mathcal{K}_b$ are restricted to a range based on the reference values. As for the electric motor for the traction purpose, the design space is strictly constrained at the lower boundary derived from the gradeability. Without losing reality, deign space of the dimensioning parameters are written as

$$\mathcal{R}_g \in [0.9, 1.1], \tag{8.6}$$

$$\mathcal{K}_b \in [40, 56], \tag{8.7}$$

$$\mathcal{T}_m \in [400, 550], \tag{8.8}$$

$$\mathcal{T}_m \in [103, 140]. \tag{8.9}$$

Approaches

Instead of the bi-level co-optimization, each dimensioning parameter is separately evaluated through VHOT, GRAB-ECO, and FACE with the discretized design space. The real-world missions are solely applied to the heavy-duty vehicles. Therefore, the investigated missions are based on real-world driving cycles, such as the Inner-City Driving Cycle ICDC and the Sub-Urban Driving Cycle SUDC (see Fig. 8.7 and 8.8).

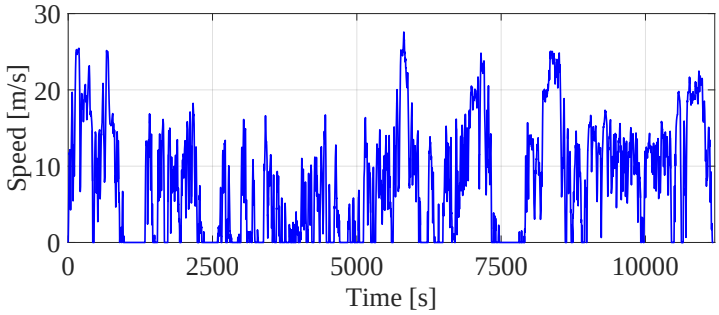

Figure 8.7 – Speed trajectory of ICDC.

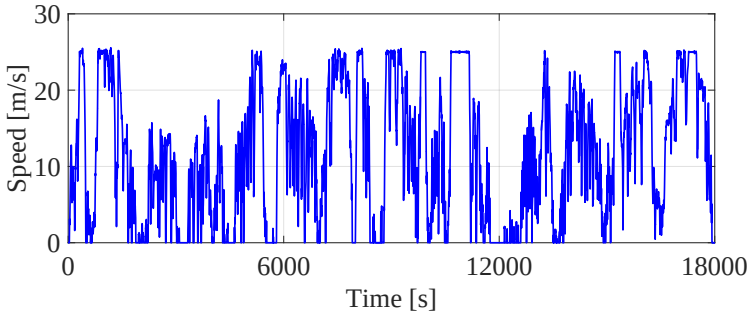

Figure 8.8 – Speed trajectory of SUDC.

8.3.3 Result and Discussion

Concerning the dimensioning parameter $\mathcal{R}_g$, it only influenced the efficiency of auxiliary power unit, but not on the vehicle performance. Fig. 8.9 summarizes the influence of $\mathcal{R}_g$

on the minimal fuel consumption over ICDC and SUDC. The fuel consumption slightly decreased as the gear ratio increased due to the efficiency increment of best-efficiency point of the auxiliary power unit.

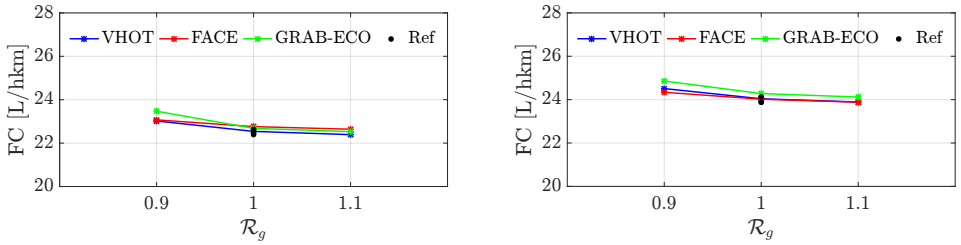

(a) ICDC (b) SUDC

Figure 8.9 – Energy consumption in function of gear ratio between engine and generator.

As shown in Fig. 8.10, battery cell number slightly reduced the minimal fuel consumption over ICDC; whereas, the impact of battery cell number on the minimal fuel consumption was negligible. However, FACE showed different prediction of the minimal fuel consumption over ICDC. Note that, the increment of battery cell number did not change the gross weight of the heavy-duty truck, but reduce the maximum allowable payload. Therefore, a smaller number of battery cells was favored in the condition that the all-electric range could meet the requirement.

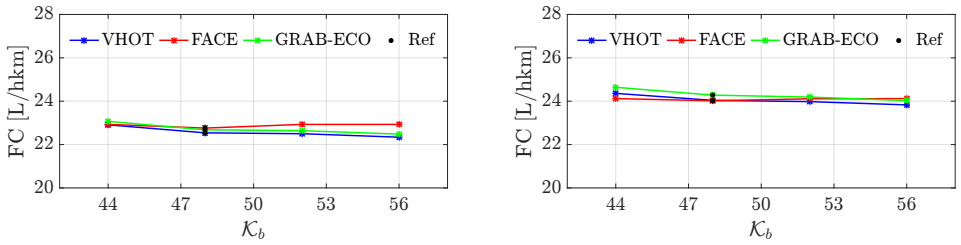

(a) ICDC (b) SUDC

Figure 8.10 – Energy consumption in function of battery cell number.

As for the traction motor, effects of the rated torque is depicted in Fig. 8.11. Over both missions, the minimal fuel consumption was significantly reduced by enlarging the rated torque of the traction motor. With the increase of the rated torque, the base speed of the traction motor decreased, leading to a squeeze of the high efficiency zone at lower motor speed, where the operating points distributed. In addition, the increment of rated torque would further enhanced the gradeability compared with the reference

series hybrid-electric truck.

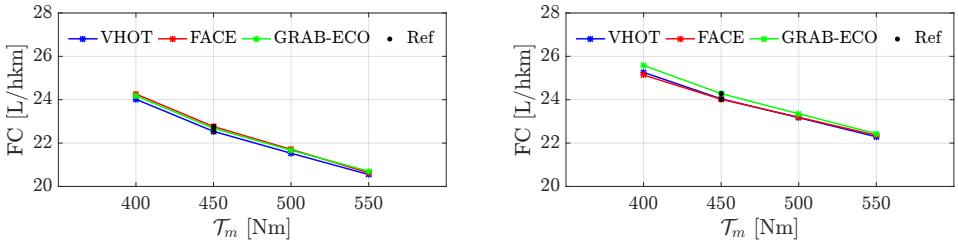

(a) ICDC (b) SUDC

Figure 8.11 – Energy consumption in function of rated torque of traction motor.

Fig. 8.12 presents the influence of the rated power of the traction motor on the minimal fuel consumption. The increment of the rated power led to an opposite effects compared with the rated torque. While maintaining the rated torque, the high efficiency zone was shifted to higher speed as the rated power increased. As a result, the average efficiency of motor operating points was reduced.

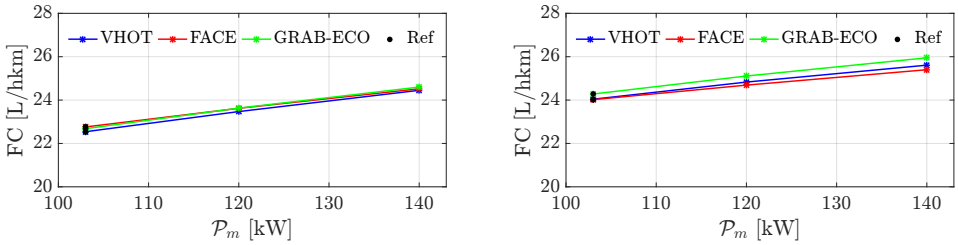

(a) ICDC (b) SUDC

Figure 8.12 – Energy consumption in function of rated power of traction motor.

Table 8.11 reports the computation time of evaluations via VHOT, SHM, and FACE over missions of ICDC and SUDC. Compared with the computation time of VHOT, GRAB-ECO reduced the computation time by orders of magnitude; whereas FACE took the least computation time.

	VHOT	GRAB-ECO	FACE
t(ICDC) [s]	634.4	15	1.05
t(SUDC) [s]	885.2	15.3	1.10

Table 8.11 – Average computation time of each function evaluation.

8.4 Co-Optimization of a Parallel Hybrid-Electric Vehicle

A parallel plug-in hybrid-electric vehicle is investigated to reduce energy consumption over given missions. Bi-level co-optimization is applied to optimize the dimensioning parameters of the reference vehicle and to investigate the impact of the different techniques of control optimization and of missions on the minimal energy consumption. In addition, the uni-level co-optimization based on FACE is implemented to optimize dimensioning parameters of powertrain components such that the energy consumption is minimized.

8.4.1 Reference Vehicle

The reference parallel hybrid-electric vehicle is a light-duty plug-in vehicle of P2 configuration, whose main features are summarized in Table 8.12.

Vehicle	m_v [kg]	1814
	R_w [m]	0.3173
	C_{v0} [N]	93.5
	C_{v1} [N/(m/s)]	5.29
	C_{v2} [N/(m/s)^2]	0.536
Engine	$\mathcal{I}_e$	SI/NA/SB
	$\mathcal{V}_e$ [L]	1.4
	$\mathcal{T}_e$ [Nm]	131
	$\mathcal{P}_e$ [kW]	60
Battery	$\mathcal{I}_b$	HP
	$\mathcal{Q}_b$ [Ah]	31
	$\mathcal{K}_b$	60
Electric Motor	$\mathcal{I}_m$	PMSM
	$\mathcal{T}_m$ [Nm]	36
	$\mathcal{P}_m$ [kW]	38
Drivetrain	$\mathcal{I}_t$	MT5
	$\mathcal{R}_m$	3.31

Table 8.12 – Main features of investigated parallel hybrid-electric vehicle.

8.4.2 Co-Optimization Problem

The co-optimization problem of powertrain design and control is briefly formulated including design constraints, the investigated dimensioning parameters, and their

resulting design space. The co-optimization problem is solved through both bi-level and uni-level co-optimization approaches.

Constraints

The vehicle performance is described in terms of two modes: the conventional and electric vehicle mode. Thus, the main design constraints are summarized as

vehicle top speed in [km/h] :	≥ 145,
vehicle top speed in [km/h] in electric mode :	≥ 55,
acceleration time to 100 in [s] :	≤ 13,
acceleration time to 50 in [s] in electric mode :	≤ 9,
gradeability in [%] :	≥ 25,
gradeability in [%] in electric mode:	≥ 13.

The dimensioning parameters to optimize are listed in $\{\mathcal{I}_e, \mathcal{V}_e, \mathcal{I}_t, \mathcal{P}_m, \mathcal{K}_b\}$, where engine technology $\mathcal{I}_e$, transmission technology $\mathcal{I}_t$, and battery cell number $\mathcal{K}_b$ are integer variables.

According to the desired top vehicle speed and acceleration time in conventional vehicle mode, the lower boundary of engine displacement of each engine technology is individually evaluated through Eq. 7.11 and 7.16. Furthermore, the lower boundary of the design space of the engine displacement is set to the minimum value of the four types of engines. However, effective penalty function will be applied to avoid violation of lower boundaries corresponding to engine types.

Despite two types of transmissions, the gear ratios are defined by the predictive analytic model of transmission in Eq. 2.24 and 2.26. The last gear is evaluated to satisfy the top vehicle speed at the engine speed of rated power; whereas the first gear meets the demanded torque for the desired gradeability.

As for the rated power of electric motor, its lower boundary is calculated to meet the requirement of acceleration time in electric mode. Moreover, the battery cell number allows the battery to provide sufficient power to the electric motor/generator.

Consequently, the resulting design space is summarized as

$$\mathcal{I}_e \in \{SI/NA/SB,\ SI/NA/LB,\ SI/TC,\ CI/TC\}, \tag{8.10}$$

$$\mathcal{V}_e \in [1.17,\ 2.65], \tag{8.11}$$

$$\mathcal{I}_t \in \{\text{MT} - 5,\ \text{MT-6}\}, \tag{8.12}$$

$$\mathcal{P}_m \in [21,\ 57], \tag{8.13}$$

$$\mathcal{K}_b \in [31,\ 100]. \tag{8.14}$$

Approaches

Bi-level co-optimization is implemented to optimize the previously mentioned dimensioning parameters. Moreover, two different techniques for powertrain control optimization are applied in the bi-level co-optimization approach, which are VHOT and SHM.

Based on FACE, the uni-level co-optimization approach is applied to optimize a single dimensioning parameter within its design space as well. Due to high nonlinearity of FACE for parallel hybrid-electric vehicles, the exhaustive search method is applied as a design optimization technique.

8.4.3 Result and Discussion

Results of several investigations on the optimization of dimensioning parameters, the impact of techniques of powertrain control, and the influences of missions are reported and discussed as follows.

Comparison with Reference Vehicle

Compared with the fuel consumption of the reference vehicle, the trajectory of fuel consumption (marked by FC) and function evaluation (denoted by K_{fcn}) through the bi-level co-optimization approach is illustrated in Fig. 8.13. As the iteration increased, the minimal fuel consumption became stabilized. The minimized fuel consumption of the optimized vehicle was reduced by 21% compared with the reference vehicle. However, the function evaluation augmented exponentially as iteration increased, thereby leading to significant increment of computation time.

Impact of Control Optimizer

Concerning the control optimization through SHM and VHOT, the trajectories of their fuel consumption and function evaluations are comparatively depicted in Fig. 8.14. The minimized fuel consumption of VHOT was slightly higher than that of SHM. Furthermore, the bi-level co-optimization via VHOT required more iterations than that through SHM under the same exit criteria of DIRECT. Yet both of them had similar number of function evaluations.

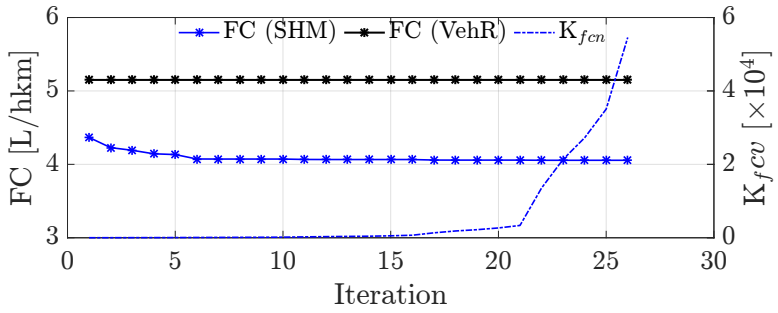

Figure 8.13 – Trajectory of bi-level co-optimization through SHM.

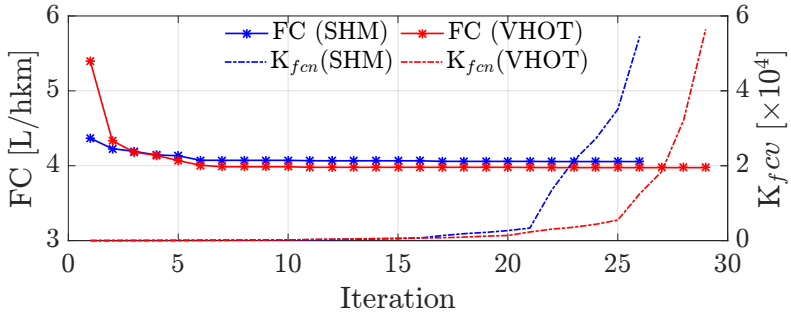

Figure 8.14 – Trajectory comparison of bi-level co-optimization through SHM and VHOT.

The detailed computational characteristics are summarized in Table 8.13. The VHOT took twice as much average time per function evaluation as SHM did. However, the average computation time of SHM was larger than the one in Chapter 4.5.2. The reason is due to extra time required to handling the data in-between two optimization levels.

	Iteration	Evaluation	CPU Time [h]	Average Time [s]
SHM	26	54568	1.77	0.1165
VHOT	29	56451	3.94	0.2511

Table 8.13 – Computational characteristics of bi-level co-optimization via SHM and VHOT.

Table 8.14 reports the dimensioning parameters of the optimized vehicle over NEDC through SHM and VHOT. Except for the type of internal combustion engine, remaining dimensioning parameters were different from each other due to different techniques of powertrain control optimization. The optimal dimensioning parameters of VehN(SHM)

were evaluated via VHOT, resulting a higher fuel consumption (4.00 L/hkm) than VehN(VHOT). The same situation occurred that VehN(SHM) had a lower fuel consumption than VehN(VHOT) evaluated through SHM. Therefore, the different optimal design parameters were caused by the implementation of the powertrain control optimization techniques.

	$\mathcal{I}_e$	$\mathcal{V}_e$ [L]	$\mathcal{I}_t$	$\mathcal{P}_m$ [kW]	$\mathcal{K}_b$
VehN(SHM)	CI/TC	1.24	MT-5	22.0	48
VehN(VHOT)	CI/TC	1.40	MT-5	23.9	54

Table 8.14 – Dimensioning parameters of optimized parallel hybrid-electric vehicles based on SHM and VHOT.

Additionally, a few relevant signals, including speed of engine and motor (ω_e and ω_m), demanded power at wheels(P_w), engine power (P_e), and state of charge of battery (marked as SOC) are comparatively depicted in Fig. 8.15 in terms of SHM and VHOT. Although the final SOC is not the same as the initial one, the difference between those two was handled in the evaluation of minimal fuel consumption by interpolation method.

Impact of Mission

The vehicle propulsion system of the reference vehicle is further optimized over extra missions, which are FTP-72 and HYWFET. The control optimization in the bi-level co-optimization approach is uniformly done through SHM.

As depicted in Fig. 8.16, fuel consumption of the optimized vehicles were compared with the reference vehicle over each investigated mission. VehN, VehF, and VehH referred to the optimized vehicles based on NEDC, FTP-72, and HYWFET, respectively. To summarize, the minimal fuel consumption was mission-dependent. Because NEDC consists of the urban and extra-urban driving condition, VehN was the good compromise among these three missions.

The percentage of tractive energy and operating time of each mode are illustrated in Fig. 8.17 for the corresponding optimized vehicles. Mode 0 indicated the standstill condition; whereas the other modes corresponded to the sequential elements in Eq. 4.38. In particular, mode 1 was the unconstrained solution; mode 2 was the pure electric mode; and mode 3 was hybrid mode that engine worked at best-efficiency condition.

Table 8.15 summarizes the computational characteristics through the bi-level co-optimization approach. Compared with the computation time of a single function evaluation in Chapter 4.5.2, the average computation time of a single function eval-

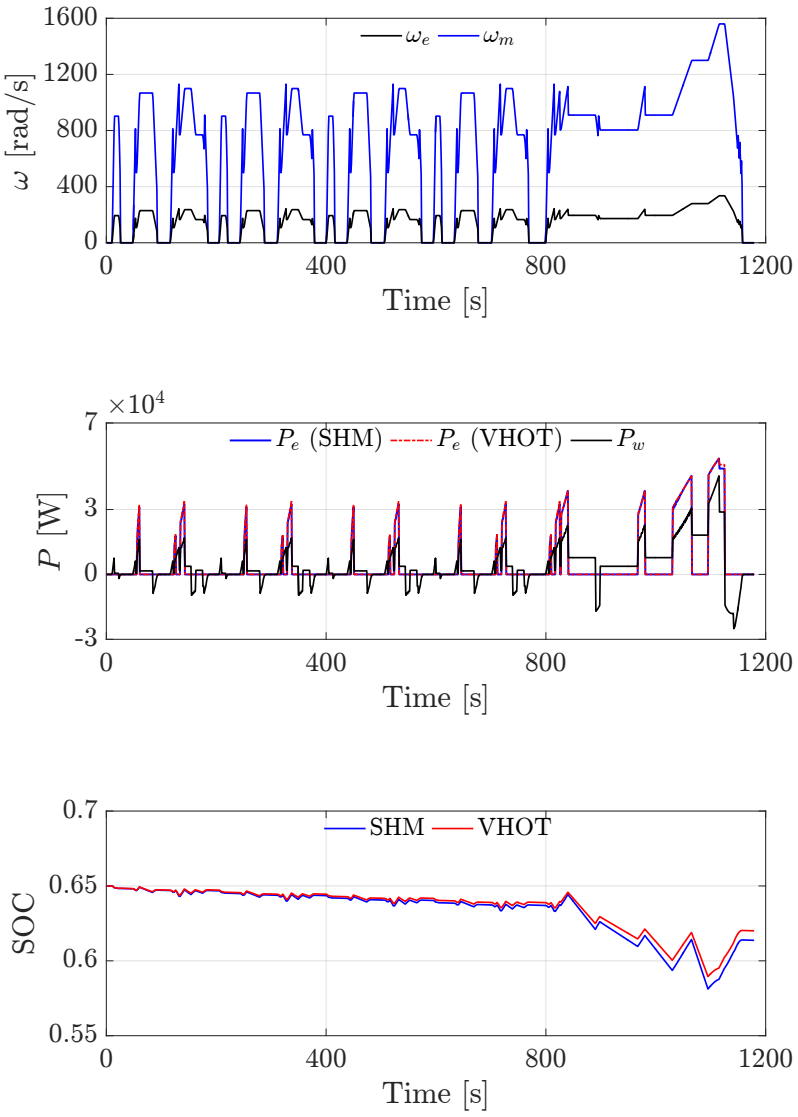

Figure 8.15 – Trajectory of relevant signals over NEDC.

uation increased over tested missions due to the data manipulation in-between two optimization levels. Moreover, the average computation time was affected by the duration of the investigated missions.

As listed in Table 8.16, the dimensioning parameters of optimized vehicles are compared with the ones of the reference vehicle. Optimal dimensioning parameters were mission-dependent. Despite the same type of transmission, the resulting gear

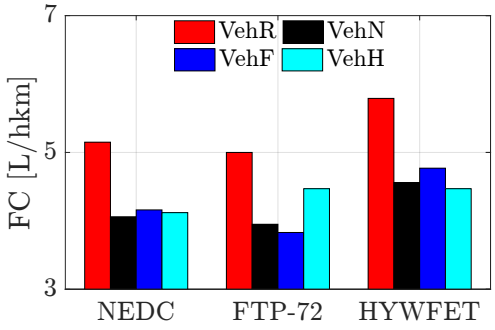

Figure 8.16 – Energy consumption of reference and optimized parallel hybrid-electric vehicles over different missions.

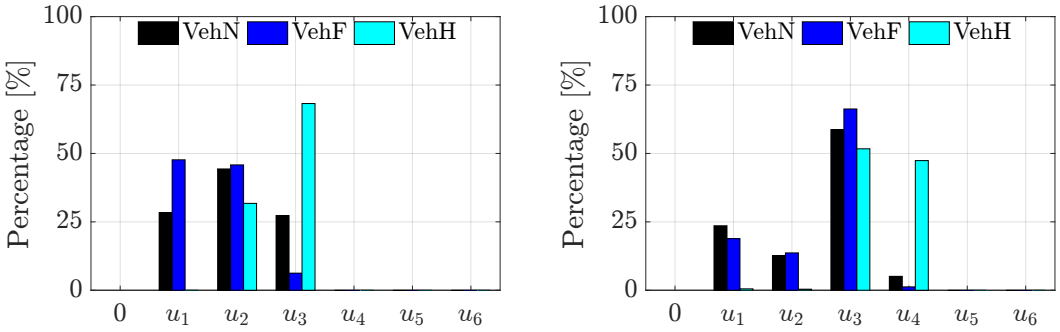

(a) tractive energy

(b) time

Figure 8.17 – Operating mode percentage in terms of time and demanded energy.

	Iteration	Evaluation	CPU Time [h]	Average Time [s]
VehN	26	54569	1.77	0.1165
VehF	27	58587	3.51	0.2163
VehH	29	112733	2.78	0.0889

Table 8.15 – Computational characteristics of bi-level co-optimization approach based on various missions.

ratios according to different engine displacements are summarized in Table 8.17. Note that, the optimized gear ratios did not take extra constraints into account.

As a consequence of the optimal dimensioning parameters, vehicle performance of each optimized vehicle is summarized in Table 8.18. Due to the restriction of the optimal gear ratio, the maximum vehicle speed in electric vehicle mode did not reach 50 km/h over HYWFET. The acceleration performance in both conventional and electric

	$\mathcal{I}_e$	$\mathcal{V}_e$ [L]	$\mathcal{T}_e$ [Nm]	$\mathcal{P}_e$ [kW]	$\mathcal{I}_t$	$\mathcal{P}_m$ [kW]	$\mathcal{K}_b$
VehR	SI/NA/SB	1.40	130	60	MT-5	38	36
VehN	CI/TC	1.24	184	60	MT-5	22	48
VehF	CI/TC	2.00	297	97	MT-5	22	48
VehH	CI/TC	1.00	149	49	MT-5	22	82

Table 8.16 – Dimensioning parameters of optimized parallel hybrid-electric vehicles based on various missions.

	$\mathcal{R}_{t1}$	$\mathcal{R}_{t2}$	$\mathcal{R}_{t3}$	$\mathcal{R}_{t4}$	$\mathcal{R}_{t5}$	$\mathcal{R}_m$
VehR	15.506	8.213	5.815	4.425	3.483	27.12
VehN	14.757	8.181	5.393	3.943	3.189	38.10
VehF	9.121	5.734	4.298	3.551	3.163	26.92
VehH	18.249	9.697	6.072	4.186	3.205	44.93

Table 8.17 – Gear ratios of optimized parallel hybrid-electric vehicles based on various missions.

vehicle mode is illustrated in Fig. 8.18.

	v_{top} [km/h]	t_{100} [s]	α [%]	$v_{top,ev}$ [km/h]	t_{50} [s]	α_{ev} [%]
VehR	137	19.89	22.92	79	7.72	10.48
VehN	150	14.10	31.59	56	9.16	12.14
VehF	151	9.44	31.59	80	10.06	8.55
VehH	144	18.05	31.59	48	NA	18.15

Table 8.18 – Performance of optimized parallel hybrid-electric vehicles based on various missions.

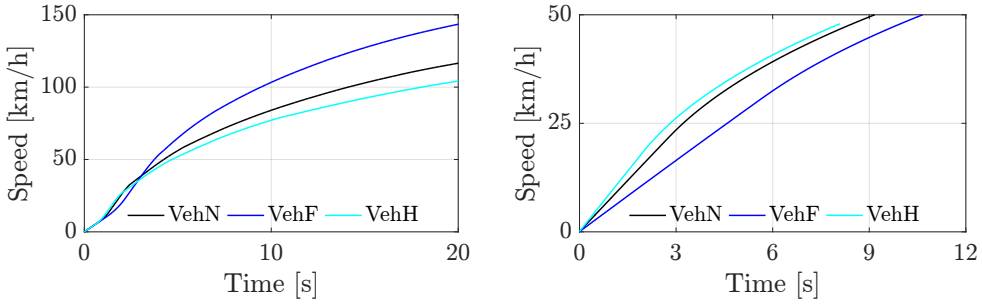

(a) from 0 to 100 km/h (b) from 0 to 50 km/h

Figure 8.18 – Acceleration performance of optimized and reference parallel hybrid-electric vehicles.

Uni-Level Co-Optimization Approach

The uni-level co-optimization is applied to optimize the dimensioning parameters of powertrain components in the reference vehicle so that the energy consumption is minimized. Due to the high nonlinearity of FACE, the full-space search method is implemented to separately optimize two dimensioning parameters, including engine displacement and capacity of battery cells.

The engine displacement is optimized within the space in Eq. 8.11. Result of the minimal fuel consumption is illustrated as a function of the engine displacement in Fig. 8.19. The minimal fuel consumption was a linear function of engine displacement, indicating downsizing of internal combustion engines was still helpful to reduce the fuel consumption. Under the same the requirement of vehicle performance, the optimum engine displacement was the smallest value and saved the most fuel.

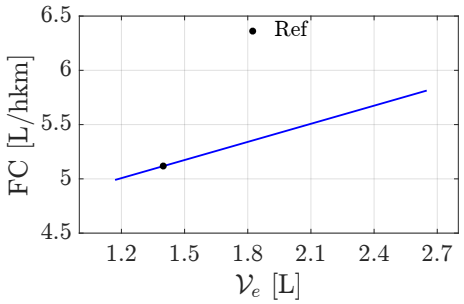

Figure 8.19 – Influence of engine displacement on fuel consumption.

The capacity of battery cells $\mathcal{Q}_b$ is investigated through the uni-level co-optimization approach. The design space of $\mathcal{Q}_b$ is from 31 to 53 Ah. As shown in Fig. 8.20, the minimum fuel consumption was achieved by the largest capacity of battery cell within its design space. The reason is simply due to the least internal resistance of the 53 Ah battery cell.

Considering the total computation time, it was about 0.4 s for the optimization of two dimensioning parameters through the uni-level co-optimization approach.

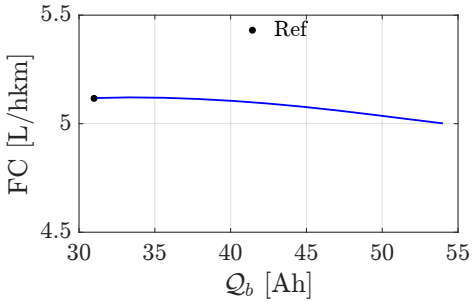

Figure 8.20 – Influence of battery cell capacity on fuel consumption.

8.5 Co-Optimization of a Parallel Hybrid-Electric Truck

In this case study, a prototype of hybrid-electric truck is optimized to reduce fuel consumption. Based on the analysis of experimental data, optimizations are performed on two aspects, which are powertrain control optimization and powertrain design optimization.

Concerning the control optimization, the minimal fuel consumption is achieved by optimal control laws with or without the consideration of the optimization of gear shift strategy. In regard with design optimization, fuel consumption is further minimized by optimizing dimensioning parameters of powertrain components.

8.5.1 Reference Vehicle

The reference truck is a parallel hybrid-electric truck in terms of P2 configuration. The main features of powertrain components are listed in Table 8.19, whereas the investigated mission is shown in Fig. 8.21.

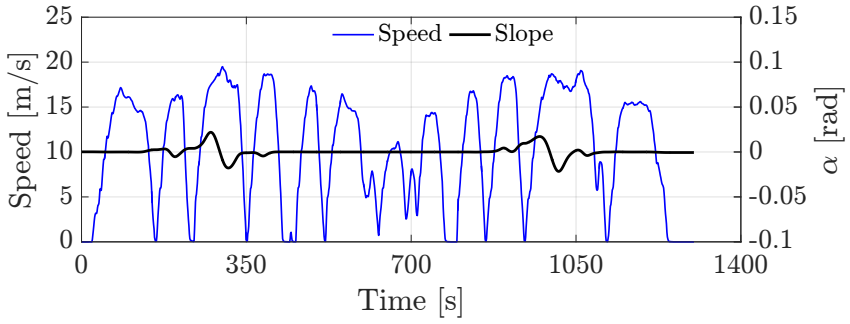

Figure 8.21 – Investigated mission for reference hybrid-electric truck.

Vehicle	m_v [kg]	17000
	R_w [m]	0.5
	$C_{ar}A_{ar}$ [m^2]	6
Engine	$\mathcal{I}_e$	CI/TC
	$\mathcal{V}_e$ [L]	9
	$\mathcal{T}_e$ [Nm]	1600
	$\mathcal{P}_e$ [kW]	235
Battery	$\mathcal{I}_b$	LiB
	$\mathcal{E}_b$ [kWh]	18
Electric Motor	$\mathcal{I}_m$	PMSM
	$\mathcal{T}_m$ [Nm]	1050
	$\mathcal{P}_m$ [kW]	150
Drivetrain	$\mathcal{I}_t$	AMT-12
	$\mathcal{R}_{fd}$	3.07

Table 8.19 – Main features of investigated parallel hybrid-electric truck.

A particular model of rolling resistance tailored for heavy-duty vehicles is implemented, which is by

$$C_{rr}(v) = C_{r,iso} + a(v^2 - v_0^2) + b(v - v_0), \tag{8.15}$$

where the speed v and v_0 are in [km/h], coefficients $C_{r,iso}$, a, and b refer to [78].

8.5.2 Co-Optimization Problem

As stated, optimization analysis of the reference hybrid-electric truck is performed at two distinct aspects: powertrain control optimization and powertrain design optimization.

Control Optimization

Control optimization is performed to benchmark the minimal fuel consumption of the reference hybrid-electric truck. The control optimization contains a single optimization of control laws splitting the power between different energy sources, and a combined optimization of control laws and gear shift strategy.

Considering the powertrain control optimization, both VHOT and SHM are implemented based on the grid-point data and predictive analytic models, respectively. Therefore, the accuracy of predictive models are cross-verified. Concerning the combined control optimization, gear shift strategy is optimized only through SHM by

enlarging the full control space in the array operation.

Design Optimization

As for the powertrain design optimization, no design constraint is applied due to the limited range of the design space compared with dimensioning parameters of real powertrain components. The investigated dimensioning parameters consist of $\left\{\mathcal{V}_e, \mathcal{I}_t, \mathcal{R}_{fd}, \mathcal{K}_b\right\}$, where transmission technology $\mathcal{I}_t$ and battery cell number $\mathcal{K}_b$ are integer variables.

The design space of engine displacement is slightly enlarged with respect to the real powertrain components, due to the high fidelity of the predictive analytic models. Thus, the design space of engine displacement is

$$\mathcal{V}_e \in [8,\ 18]. \tag{8.16}$$

The design space of the transmission technological parameter is

$$\mathcal{I}_t \in \{\text{AMT-12, AMT-14}\}, \tag{8.17}$$

where AMT-12 stands for automated manual transmission of 12 speeds, and AMT-14 for that of 14 speeds.

As for the ratio of final drive, the design space is

$$\mathcal{R}_{fd} \in [2.5,\ 4.9], \tag{8.18}$$

where boundary values are collected from public available brochures of Scania's trucks.

The design space of battery cell number is evenly deviated based on the one of reference vehicle.

The bi-level co-optimization approach is used to optimize the dimensioning parameters of powertrain components through the combination of DIRECT and SHM.

8.5.3 Result and Discussion

Comparison of VHOT and SHM

The minimal fuel consumption of the reference vehicle evaluated by VHOT is based on the original data of powertrain components; whereas SHM evaluates the minimal fuel consumption based on analytic models of powertrain components. Fig. 8.22 shows the minimized fuel consumption evaluated based on VHOT and SHM. The discrepancy of

the minimized fuel consumption was about 0.35 L/hkm (about 1.9%). Therefore, SHM was capable of minimizing fuel consumption.

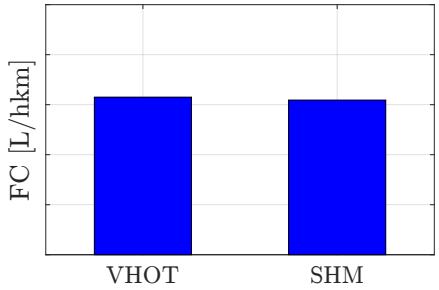

Figure 8.22 – Minimal fuel consumption of the reference hybrid-electric truck.

Minimization of Fuel Consumption through Control Optimization

Considering different control optimizations, the minimized fuel consumption is comparatively illustrated in Fig. 8.23. The fuel consumption of the reference vehicle was denoted by REF; whereas EMO and GSO indicate the minimal fuel consumption evaluated with optimal energy management strategy, and the combined optimal energy management with the optimal gear shift, respectively. The improvements of EMO and GSO on the fuel consumption corresponded to about 33% and 41% compared with the reference vehicle. A further improvement of 7% on fuel consumption was obtained by adding optimal gear shift strategy.

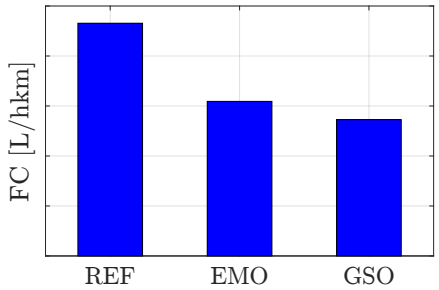

Figure 8.23 – Minimized fuel consumption of different powertrain control optimizations.

Additionally, the cumulative electrochemical power of battery is presented in Fig. 8.24. The final varied electrochemical energy was required to be the same as the reference one. Despite slight differences between the optimized final energy and the

reference one, the minimized fuel consumption had accounted for the difference of varied electrochemical energy of battery.

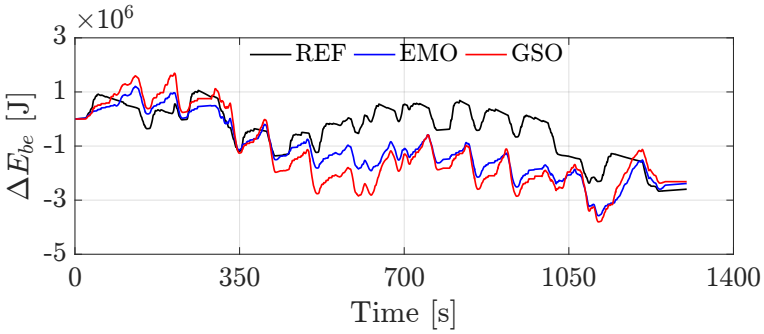

Figure 8.24 – Trajectory of varied electrochemical energy of battery over investigated mission.

The optimized gear shift schedule obtained through the gear shift optimization (GSO) is presented in Fig. 8.25. The highest gear number in the optimized gear shift schedule was less frequently used compared with that in the reference vehicle.

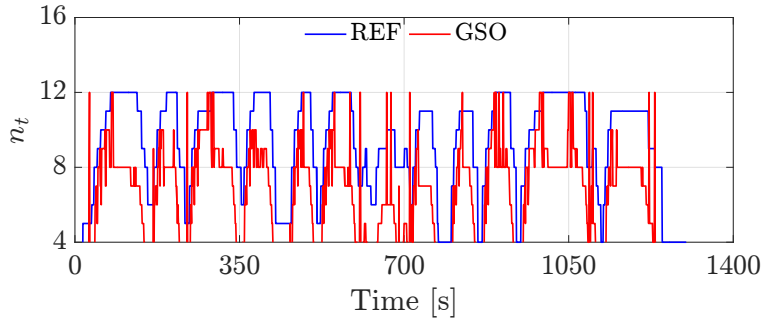

Figure 8.25 – Optimized gear shift schedule over the mission.

Fig. 8.26 shows the comparison of the operating points of the engine based on reference data, single energy management optimization, and combined optimization with optimal gear shift schedule. As optimization level increased, the operating points of the internal combustion engine were shifted to concentrate on the higher efficiency area. Compared with reference data, energy management optimization removed the operating points at boundaries. Moreover, the gear shift optimization centralized operating points at the highest efficiency zone.

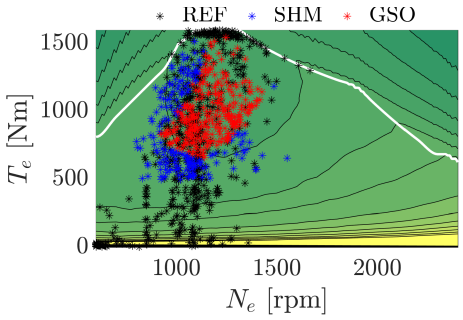

Figure 8.26 – Operating points of internal combustion engine on its fuel consumption map.

Minimization of Fuel Consumption through Design Optimization

In the bi-level co-optimization approach, the dimensioning parameters of powertrain components are optimized to further reduce fuel consumption. However, the electric motor/generator is always maintained the same in the investigation of powertrain design optimization.

As shown in Fig. 8.27, the fuel consumption of optimized powertrain and the one of gear shift optimization are compared with the reference vehicle. Slight reduction of fuel consumption was achieve by the powertrain optimization, which was about 1.6%.

The optimal dimensioning parameters are summarized in Table 8.20. The optimal battery cell number was the upper boundary of its design space. The improvement on battery was not significant because of its high efficiency and the limited design space. As the engine downsized and the operating points shifted, the fuel consumption was further reduced through powertrain design optimization.

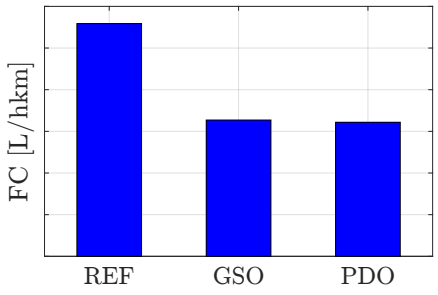

Figure 8.27 – Minimized fuel consumption of powertrain control and design optimizations.

	$\mathcal{V}_e$ [L]	$\mathcal{I}_t$	$\mathcal{R}_{fd}$
Reference	9.3	AMT-12	3.07
Optimized	8.0	AMT-14	4.34

Table 8.20 – Dimensioning parameters of optimized hybrid-electric truck.